Quasiparticles in d-wave superconductors within density functional theory

2001 J. Phys.: Condens. Matter 13 8625

(http://iopscience.iop.org/0953-8984/13/38/307)

INSTITUTE OF PHYSICS PUBLISHING JOURNAL OF PHYSICS: CONDENSED MATTER

J. Phys.: Condens. Matter **13** (2001) 8625–8652 PII: S0953-8984(01)24873-5

Quasiparticles in d-wave superconductors within density functional theory

Z Szotek[1], B L Gyorffy[2], W M Temmerman[1], O K Andersen[3] and O Jepsen[3]

[1] Daresbury Laboratory, Daresbury, Warrington WA4 4AD, UK
[2] H H Wills Physics Laboratory, University of Bristol, Tyndall Avenue, Bristol BS8 1TL, UK
[3] Max-Planck-Institut für Festkörperforschung, Postfach 800665, D-70506, Stuttgart, Germany

Received 17 May 2001
Published 7 September 2001
Online at stacks.iop.org/JPhysCM/13/8625

Abstract

We present a semiphenomenological approach to calculating the quasiparticle spectra of high-temperature superconductors. It is based on a particularly efficient parametrization of the effective electron–electron interaction afforded by the density functional theory for superconductors and a tight-binding linearized-muffin-tin-orbital scheme for solving the corresponding Kohn–Sham–Bogoliubov–de Gennes equations. We apply this methodology to $YBa_2Cu_3O_{7-\delta}$ (YBCO) and illustrate its potential by investigating a number of site- and orbital-specific, but otherwise phenomenological, models of pairing in quantitative detail. We compare our results for the anisotropy of the gap function on the Fermi surface with those deduced from photoemission experiments on single crystals of YBCO. Also, the low-temperature specific heat and penetration depth are calculated and compared with measurements. We investigate the doping dependence of the superconducting gap, transition temperature, T_c, and penetration depth. We present new evidence that the Van Hove-like scenario is an essential feature of superconductivity in the cuprate superconductors. Since our description of pairing is phenomenological, we shed new light on the physical mechanism of pairing only indirectly and conclude, provisionally, that the dominant pairing interaction operates between electrons of opposite spins, on nearest-neighbour Cu sites in $d_{x^2-y^2}$ orbitals.

1. Introduction

The phenomenon of the high-temperature superconductivity (HTS), discovered over a decade ago by Bednorz and Müller [1], has stimulated an unprecedented theoretical and experimental effort directed towards discovery of the pairing mechanism in these systems. Unfortunately, despite all the progress made, the origin of the attractive force, responsible for the formation of the Cooper pairs in these complicated materials, is still unknown. The complexity of

cuprates, both in their normal and superconducting states, is no doubt going to attract interest for many more years to come. In this paper, instead of speculating on the microscopic nature of the pairing, we concentrate on reviewing our results for a variety of superconducting properties of YBCO, calculated on the basis of the quasiparticle spectra obtained within a semiphenomenological approach, combining first-principles electronic structure with a phenomenological pairing potential [2–6]. Our approach has been formulated within density functional theory (DFT) for superconductors [7, 8], and its basic equations are of the Bogoliubov–de Gennes form. They are obtained from the so-called eight-band model Hamiltonian [9], by augmenting it with a phenomenological pairing potential. The central quantity of this approach is an *electron–electron interaction kernel* $K(\boldsymbol{r}_1, \boldsymbol{r}'_1; \boldsymbol{r}_2, \boldsymbol{r}'_2)$ which, when attractive, leads to superconductivity. This interaction kernel is parametrized by a set of interaction constants $K_{RL,R'L'}$, with R, R' and L, L' referring to the positions and orbital character, respectively, of the two electrons. These interaction constants $K_{RL,R'L'}$ are treated as adjustable parameters of the theory, and combined with the pairing amplitude, the order parameter of the theory, give rise to the phenomenological pairing potential. It is the consequences of this semiphenomenological approach for superconductivity of HTS materials that we are concerned with in this paper. If a specific coefficient $K_{RL,R'L'}$, with all the others set equal to zero, can be adjusted to give a good quantitative account of the quasiparticle spectrum in the superconducting state of a particular superconductor, then we shall conclude, with appropriate caution, that the attraction operates between electrons in orbitals RL and $R'L'$. Thus, indirectly we can shed light on the mechanism of pairing operating in the cuprate superconductors.

In the remainder of the paper we outline briefly the underlying equations of the density functional theory for superconductors (DFTS), and introduce the phenomenological pairing potential, which will be incorporated into the eight-band model Hamiltonian [9], providing a good quantitative description of the first-principles LDA band structure of YBCO, in the normal state, within 2 eV of the Fermi energy ε_F. The local orbitals of the eight-band model provide the basis for the parametrization of the interaction kernel, and we shall briefly describe the approximations involved and the possible pairing scenarios that arise as a result of this parametrization. Since our aim is to study the consequences of this methodology in confronting experimental evidence, in the remaining sections of the paper we review our results for the superconducting gap, low-temperature specific heat, penetration depth, and T_c, both at optimal doping and as a function of doping. We finalize the paper by drawing conclusions from this work.

2. Density functional theory and Bogoliubov–de Gennes equations

The formal framework of the DFT for superconductors was developed by Oliveira, Gross, and Kohn [7, 8], in close analogy to the DFT for spin-polarized systems (SP-DFT) [10, 11]. The corresponding Kohn–Sham equations have the form of the Bogoliubov–de Gennes (BdG) equations [2, 12], which are a set of coupled integral equations

$$\begin{aligned}\left(-\frac{1}{2}\nabla^2 + V(\boldsymbol{r}) - \mu\right)u_j(\boldsymbol{r}) + \int \Delta(\boldsymbol{r}, \boldsymbol{r}')v_j(\boldsymbol{r}')\,\mathrm{d}^3r' &= E_j u_j(\boldsymbol{r}) \\ -\left(-\frac{1}{2}\nabla^2 + V(\boldsymbol{r}) - \mu\right)v_j(\boldsymbol{r}) + \int \Delta^*(\boldsymbol{r}, \boldsymbol{r}')u_j(\boldsymbol{r}')\,\mathrm{d}^3r' &= E_j v_j(\boldsymbol{r})\end{aligned} \tag{1}$$

that have to be solved self-consistently with respect to the chemical potential, μ, the one-electron effective potential, V, the pairing potential, Δ, and the pairing amplitude χ, the

order parameter of the theory. Note that within the present formulation of DFTS only the singlet pairing is considered, i.e., only electrons of opposite spins and momenta $(k\uparrow, -k\downarrow)$ are allowed to pair.

The one-electron effective potential V (assumed to be independent of spin) is defined by the usual relation

$$V(\boldsymbol{r}) = V_{\mathrm{ext}}(\boldsymbol{r}) + \int \frac{n(\boldsymbol{r}')}{|\boldsymbol{r} - \boldsymbol{r}'|}\, \mathrm{d}^3 r' + \frac{\delta \Omega_{\mathrm{xc}}[n, \chi]}{\delta n(\boldsymbol{r})} \tag{2}$$

and the pairing potential

$$\Delta(\boldsymbol{r}, \boldsymbol{r}') = \frac{\delta \Omega_{\mathrm{xc}}[n, \chi]}{\delta \chi(\boldsymbol{r}, \boldsymbol{r}')} \tag{3}$$

is a functional derivative of the XC free-energy functional with respect to the pairing amplitude χ. Note that in the DFTS the exchange–correlation (XC) free energy is a functional of the electron charge density n and pairing amplitude χ. If Δ was equal to zero, the BdG equations would split into two separate equations, one for electrons and one for holes.

Although, like in any DFT, the solutions of the BdG equations, namely the amplitudes u_j and v_j, and the corresponding eigenvalues E_j, are only auxiliary quantities whose sole purpose is to provide representation for calculating the electron charge density n:

$$n(\boldsymbol{r}) = 2 \sum_j \left[1 - f(E_j)\right] \left|v_j(\boldsymbol{r})\right|^2 + f(E_j) \left|u_j(\boldsymbol{r})\right|^2 \tag{4}$$

and pairing amplitude χ:

$$\chi(\boldsymbol{r}, \boldsymbol{r}') = \sum_j \left[1 - f(E_j)\right] u_j(\boldsymbol{r}) v_j^*(\boldsymbol{r}') - f(E_j) u_j(\boldsymbol{r}') v_j^*(\boldsymbol{r}) \tag{5}$$

we shall interpret them provisionally as elementary excitations of the superconducting state (i.e. the quasiparticle spectrum of the superconducting state), and regard u_j as the amplitude for such an elementary excitation being a quasiparticle and v_j as being the amplitude of a quasihole. Here $f(E) \equiv [1 + \exp(E/k_B T)]^{-1}$ is the Fermi function, and the normalization of the eigenfunctions is such that

$$\int \left|u_j(\boldsymbol{r})\right|^2 \, \mathrm{d}^3 r + \int \left|v_j(\boldsymbol{r})\right|^2 \, \mathrm{d}^3 r = 1. \tag{6}$$

The effective quasiparticle spectrum $E_\nu(\boldsymbol{k})$ of the BdG equation, with ν being the band index and $\boldsymbol{k}$ a wave vector in the first Brillouin zone (BZ), may be thought of as the normal-state single-electron spectrum $\varepsilon_\nu(\boldsymbol{k})$, doubled up by folding around the chemical potential μ, and subsequently split by the pairing potential Δ. Therefore, the solutions come in pairs: a set of positive eigenvalues, $E_\nu^+(\boldsymbol{k})$, and a set of negative eigenvalues, $E_\nu^-(\boldsymbol{k})$, that are exactly symmetrical with each other about the chemical potential. Only the positive eigenvalues are physically meaningful but, for the sake of calculations, one can use the negative eigenvalues and the corresponding eigenvectors and interpret the results without loss of generality.

Based on the BdG quasiparticle spectrum, and following Suvasini *et al* [12], we can define the superconducting gap as

$$2\Delta_\nu(\boldsymbol{k}_{\mathrm{F}}) \equiv \left|E_\nu^+(\boldsymbol{k}_{\mathrm{F}}) - E_\nu^-(\boldsymbol{k}_{\mathrm{F}})\right| = 2\left|E_\nu^+(\boldsymbol{k}_{\mathrm{F}})\right|$$

where $\boldsymbol{k}_{\mathrm{F}}$ is a vector corresponding to a point on the νth sheet of a pseudo-Fermi surface defined by

$$\sum_L \left|u_{L,\nu}^{\boldsymbol{k}_{\mathrm{F}}}\right|^2 = \sum_L \left|v_{L,\nu}^{\boldsymbol{k}_{\mathrm{F}}}\right|^2$$

i.e. where $|\chi^{\boldsymbol{k}}| = 1/2$.

Using the self-consistent solutions of the BdG equations, in this paper we calculate a variety of superconducting properties of the cuprate superconductors, and compare them with experiments in section 5.

The pairing potential is electronic in nature, because it arises from electron correlations. It is static (no time or energy dependence). Therefore, within the present formulation no retardation effects are possible. Dynamic effects can only be treated in an average way, to the extent that it is possible to represent them in terms of an electronic interaction. To consider the interaction with phonons one needs a two-density theory, where both electrons and ions are treated on the same footing [13]. Since there still exists no usable form of Ω_{xc} it is helpful to rewrite the differential equation for the pairing potential in an equivalent integral form:

$$\Delta(\boldsymbol{r}_1, \boldsymbol{r}_1') = \int\int K(\boldsymbol{r}_1, \boldsymbol{r}_1'; \boldsymbol{r}_2, \boldsymbol{r}_2')\chi(\boldsymbol{r}_2, \boldsymbol{r}_2')\, \mathrm{d}^3 r_2\, \mathrm{d}^3 r_2' \tag{7}$$

with

$$K(\boldsymbol{r}_1, \boldsymbol{r}_1'; \boldsymbol{r}_2, \boldsymbol{r}_2'[n, \chi]) \equiv \frac{\delta^2 \Omega_{xc}[n, \chi]}{\delta\chi(\boldsymbol{r}_1, \boldsymbol{r}_1')\, \delta\chi(\boldsymbol{r}_2, \boldsymbol{r}_2')} \tag{8}$$

being the pair interaction kernel. In the most general case, K is also a functional of n and χ. However, since the mechanism of pairing is not known there is no way of evaluating this pair interaction kernel from first principles. Therefore, in order to make the theory useful for the high-T_c cuprates, we shall have to introduce some approximations. Fortunately, the DFT allows for a very efficient parametrization of the kernel in terms of the local orbitals of the theory and treating the resulting orbital and site-dependent quantities as adjustable parameters, whose values can be determined by fitting to the experimental quantities.

With respect to the formula for the pairing potential it can be further simplified in a manner similar to the corresponding relation in the SP-DFT between the exchange potential and the magnetization via the exchange interaction kernel I:

$$V_\uparrow(\boldsymbol{r}_1) - V_\downarrow(\boldsymbol{r}_1) = \int I(\boldsymbol{r}_1, \boldsymbol{r}_2) m(\boldsymbol{r}_2)\, \mathrm{d}^3 r_2 \approx I(\boldsymbol{r}_1) m(\boldsymbol{r}_1)$$

which by implementing a local approximation can be transformed into a simple Stoner relation. And this is what we shall implement also in the study for the superconducting state.

3. Tight-binding representation

To implement the methodology described above and facilitate the said parametrization of the pair interaction kernel, we expand the single-particle wave function in terms of the local tight-binding muffin-tin orbitals $\phi_L(r - R)$:

$$\begin{bmatrix} u_\nu(\boldsymbol{r}) \\ v_\nu(\boldsymbol{r}) \end{bmatrix} = \sum_{RL} \varphi_L(\boldsymbol{r} - \boldsymbol{R}) \begin{bmatrix} u_{RL,\nu} \\ v_{RL,\nu} \end{bmatrix}. \tag{9}$$

As before, R labels the site ($\boldsymbol{R}$) and L the shape (e.g. atom and angular momentum type) of the orbital. Consequently, in this local tight-binding representation the BdG equations take the following matrix form:

$$\sum_{RL} \begin{bmatrix} H_{R'L',RL} - (\mu + E_\nu) O_{R'L',RL} & \Delta_{R'L',RL} \\ \Delta^*_{RL,R'L'} & -H_{R'L',RL} + (\mu - E_\nu) O_{R'L',RL} \end{bmatrix} \begin{bmatrix} u_{RL,\nu} \\ v_{RL,\nu} \end{bmatrix} = \begin{bmatrix} 0 \\ 0 \end{bmatrix} \tag{10}$$

with the matrix elements of the Hamiltonian and the overlap matrix given by the integrals over the unit cell

$$H_{R'L',RL} \equiv \int \varphi^*_{L'}(\boldsymbol{r}-\boldsymbol{R}')\left[-\frac{1}{2}\nabla^2 + V(\boldsymbol{r})\right]\varphi_L(\boldsymbol{r}-\boldsymbol{R})\,\mathrm{d}^3r$$

$$O_{R'L',RL} \equiv \int \varphi^*_{L'}(\boldsymbol{r}-\boldsymbol{R}')\varphi_L(\boldsymbol{r}-\boldsymbol{R})\,\mathrm{d}^3r$$

and the integral equation for the pairing potential acquiring the following form:

$$\Delta_{R_1L_1,R_1'L_1'} = \sum_{R_2L_2}\sum_{R_2'L_2'} K_{R_1L_1,R_1'L_1';R_2L_2,R_2'L_2'}\chi_{R_2L_2,R_2'L_2'}. \tag{11}$$

To make the above relation between the pairing potential and pairing amplitude useful, we have to evaluate the unknown coefficients, $K_{R_1L_1,R_1'L_1';R_2L_2,R_2'L_2'}$, of the pair interaction kernel. This four-point function describes the scattering of an $(\uparrow,\downarrow)$ pair of electrons in orbitals R_2L_2 and $R_2'L_2'$ into an $(\uparrow,\downarrow)$ pair in orbitals R_1L_1 and $R_1'L_1'$ (and similarly for the $(\downarrow,\uparrow)$ pair). To make progress, first we have to abandon hope of evaluating K from first principles, and drop its functional dependence on n and χ. Then we assume that the kernel is local:

$$K_{R_1L_1,R_1'L_1';R_2L_2,R_2'L_2'} = \delta_{R_1R_2}\delta_{L_1L_2}\delta_{R_1'R_2'}\delta_{L_1'L_2'}K_{R_1L_1,R_1'L_1'} \tag{12}$$

meaning that K vanishes unless all spin-up electrons are in the same orbital and similarly for the spin-down electrons. This local representation of the interaction kernel results in a simple, Stoner-like, relation between the pairing potential and pairing amplitude

$$\Delta_{RL,R'L'} = K_{RL,R'L'}\chi_{RL,R'L'}. \tag{13}$$

It states that in the local orbital representation each matrix element of the pairing potential is proportional to the corresponding matrix element of the pairing amplitude, and is independent of all the other components. Of course, the matrix elements of the pair interaction kernel are still unknown. At this point, therefore, we make a further approximation, namely we shall treat these coefficients as adjustable parameters of the theory. The hope of this strategy is that a small number of these coefficients will suffice to produce agreement with a large number of experimental data. In fact in most of our studies we pick just one of these coefficients to be non-zero and fix its value by requiring that the calculated T_c agrees with the experimental evidence. Then given the first-principles aspect of our theory (in relation to the normal-state electronic structure), all calculated superconducting properties, other than T_c, will be predictions of the theory and will be calculated without additional adjustable parameters. This strategy gives rise to a variety of pairing scenarios [3] where one can choose various orbitals to assign electrons to, determine the strength of the coupling parameter K by fitting to the experimental T_c, and study the consequences regarding a large number of superconducting properties. The aim is to identify the pairing scenario that agrees with most properties and experiments.

The final point that we would like to make before leaving this section is that in the actual calculations, we shall replace the Hamiltonian matrix, appearing in the above TB-BdG equations, by the eight-band model derived from the full first-principles LDA Hamiltonian [9]. Moreover, we shall not update the tight-binding parameters of this model during the self-consistency cycles, which will make our methodology a weak-coupling theory. At every iteration we shall only update the chemical potential, the pairing potential, and the pairing amplitude.

4. Electronic structure of $YBa_2Cu_3O_7$ and eight-band model

Before introducing the eight-band model for YBCO, in figure 1 we summarize the full electronic and structural information on the optimally doped compound. As can be seen

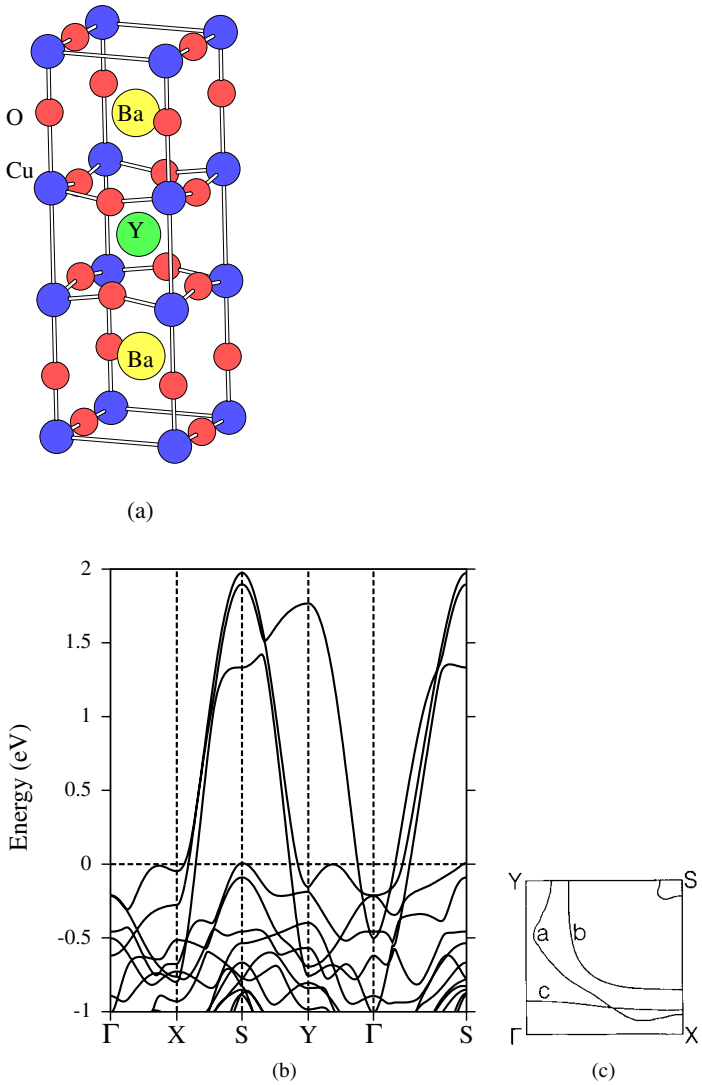

Figure 1. (a) The crystal structure of $YBa_2Cu_3O_7$. Y, in the middle of the orthorhombic unit cell, separates the two copper–oxygen planes. The copper–oxygen chains run along the edges of the unit cell. Ba lies between the planes and the chains. (b) The electronic structure of $YBa_2Cu_3O_7$ between the $k_\parallel$-points $(0, 0)$, $(\pi/a, 0)$, $(\pi/a, \pi/b)$, $(0, \pi/b)$, $(0, 0)$, $(\pi/a, \pi/b)$ in the $k_z = 0$ plane of the orthorhombic Brillouin zone as calculated by the full-potential LMTO method and using the local density functional theory. (c) Intersection of the Fermi surface of $YBa_2Cu_3O_7$ with the $k_z = 0$ plane of the orthorhombic Brillouin zone as calculated by the full-potential LMTO method using the local density functional theory. The coordinates are for Γ: $(0, 0)$; X: $(\pi/a, 0)$; S: $(\pi/a, \pi/b)$; and Y: $(0, \pi/b)$.

in figure 1(a), the optimally doped YBCO crystallizes in the orthorhombic structure whose most prominent feature is a set of CuO_2 planes which are dimpled, meaning that the oxygens occupy slightly out-of-plane positions. The CuO_2 planes are arranged in pairs (bilayer), as mirror reflections of each other with respect to the yttrium [001] plane. The CuO_2 planes are a generic feature of the high-T_c cuprates and, as such, are of particular interest for the present

study. Another important feature of YBCO is a CuO chain which, however, is not a generic feature of HTSs. All these structural features are reflected in the presented LDA band structure (figure 1(b)), giving rise to the Fermi surface displayed in figure 1(c).

The band structure features the anti-bonding (of CuO_2 planes) pdσ bands, with a total width of about 10 eV, and a chain-related band, crossing the Fermi level, here marked by energy zero. The strongly hybridized anti-bonding pdσ band has a maximum at the S point and a minimum at the Γ point. It exhibits a set of bifurcated saddle points near the X and Y symmetry points. These bifurcated saddle points give rise to a logarithmic Van Hove singularity (VHS) in the density of states. As can be seen in figure 1(c) for the basal plane, the Fermi surface of YBCO consists of four sheets. The main cross-sections of the Fermi surface, marked 'a' and 'b', originate from the CuO_2 planes, while the sheet marked 'c' is chain-related. The smallest element of the Fermi surface, situated around the S point, the so-called stick, is due to BaO layers. This FS has been verified experimentally, except that the saddle points observed by angle-resolved photoemission spectroscopy (ARPES) appear to be extended, while the LDA calculations give the bifurcated saddle points [14].

This complex band structure of figure 1(b) was used by Andersen *et al* to derive the so-called eight-band model Hamiltonian [9]. The motivation for deriving the eight-band model was to represent faithfully, with a minimal set of orbitals, generic features of the electronic structure of cuprates, i.e., those originating from CuO_2 planes. The bands derived from the non-generic structural elements, separating the CuO_2 layers, such as the chain and BaO layers, have been removed. As a consequence, the eight-band model is two dimensional. It features eight orthonormal local orbitals φ_L ($L = 1$ to 8) per CuO_2 plane (layer). The first four of these are the σ-orbitals: O2 p_x, Cu $d_{x^2-y^2}$, O3 p_y, and Cu s. The others are the π-orbitals: O2 p_z, Cu d_{xz}, O3 p_z, and Cu d_{yz}. The Cu s orbital is the most diffuse and provides most of the hopping perpendicular to the layer and, hence, is mostly responsible for the splitting of the two conduction bands in a bilayered material into even and odd bands (a bilayer has 16 orbitals) (figure 2). This eight-band, orthonormal, nearest-neighbour, tight-binding Hamiltonian

$$H^{\boldsymbol{k}}_{L'L} = \delta_{L'L}\varepsilon_L + \sum_{\boldsymbol{T}} t_{\boldsymbol{0}L',\boldsymbol{T}L} \exp(\mathrm{i}\boldsymbol{k}\cdot\boldsymbol{T}) \qquad \text{with } O^{\boldsymbol{k}}_{L'L} = \delta_{L'L}$$

describes accurately the LDA bands within ± 1 eV around the Fermi level. The hopping integrals, $t_{\boldsymbol{0}L',\boldsymbol{T}L}$, and site energies, ε_L, have been determined by fitting to the self-consistent LDA calculation.

The advantage of using the eight-band model, over e.g. the one- or three-band models, lies in the feature that we are dealing with physical orbitals to which we can assign electrons. In this way we can study a variety of pairing scenarios that can we hope provide us with further insights into a possible origin of the pairing mechanism.

In figure 2 we summarize the electronic structure that the eight-band model gives rise to. Remember that the eight-band model was derived to represent accurately the generic features of the electronic structure of high-T_c materials, i.e., those that originate from CuO_2 planes. Indeed the band structure along the main crystallographic directions in the 2D BZ shows the two pdσ bands which in the language of the eight-band model are referred to as the odd and even bands (see figure 2(a)). The odd bands show, very close to the Fermi level, the characteristic bifurcated saddle points at X and Y symmetry points, which give rise to the VHS in the density of states (DOS) (figure 2(b)). Note that the VHS is only about 2 meV below the Fermi level, and that due to slight orthorhombicity of the crystal structure, there are two VHS peaks, separated by about 8 meV. The jump in the DOS at about 14 meV reflects the electron pockets at the X and Y points (since the energy at the X and Y points is lower; therefore the DOS jumps). The FS of the eight-band model, shown in figure 2(c), features the two main sheets, even and odd, originating from the corresponding even and odd bands, crossing the

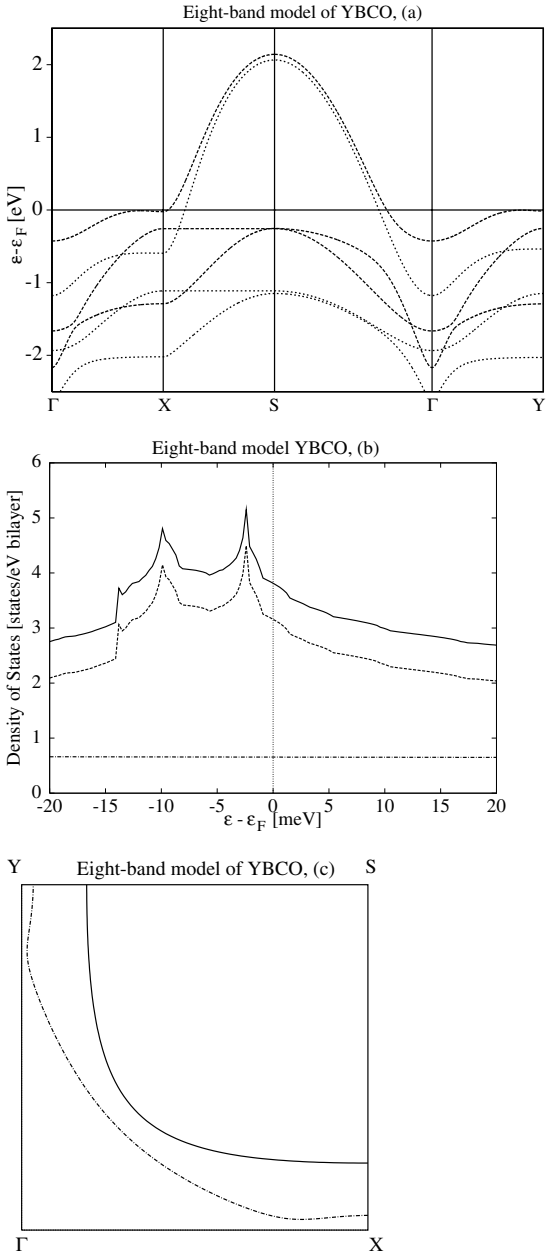

Figure 2. (a) The energy bands of the eight-band model of a CuO_2 bilayer of $YBa_2Cu_3O_7$ along the symmetry lines in the two-dimensional Brillouin zone. The dashed curves refer to the eight odd (anti-bonding between the layers) bands and the dotted curves to the eight even (bonding) bands. (b) The normal-state density of states in the neighbourhood of the Fermi level for the eight odd (dashed curve) and eight even (chain curve) plane bands of $YBa_2Cu_3O_7$, as well as their sum (full curve). The two logarithmic Van Hove singularities are due to the saddle points of the odd plane band near respectively X and Y. (c) The odd (chain curve) and even (full curve) sheets of the Fermi surface of a CuO_2 bilayer of $YBa_2Cu_3O_7$ in the irreducible part of the two-dimensional Brillouin zone. It is this part of the electronic structure which the eight-band model is designed to reproduce accurately.

Fermi level. All the evidence presented in this figure is very convincing as regards the assertion that the eight-band model does represent well this part of the electronic structure of the high-T_c cuprates that matters for superconductivity.

5. Results

5.1. Pairing scenarios and the corresponding superconducting gaps

As mentioned before, our methodology enables a study of various pairing scenarios where electrons in different orbitals and/or sites are coupled by an attractive interaction. In figure 3, we have depicted five different pairing scenarios of s- and d-type symmetries. The convention

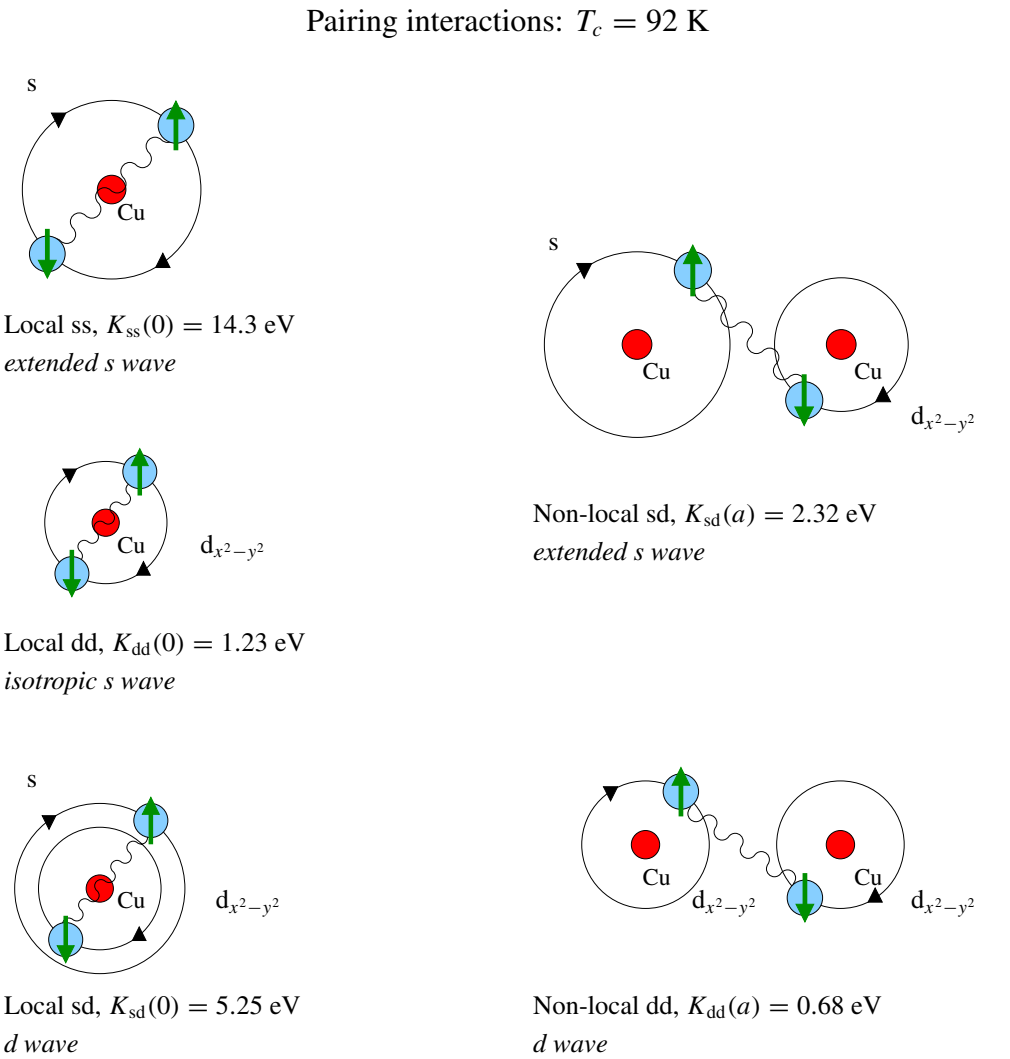

Figure 3. Schematic diagrams depicting scenarios studied for various pairing interactions, operating between Cu s and Cu $d_{x^2-y^2}$ orbitals in the CuO_2 layers. Details are given in the text.

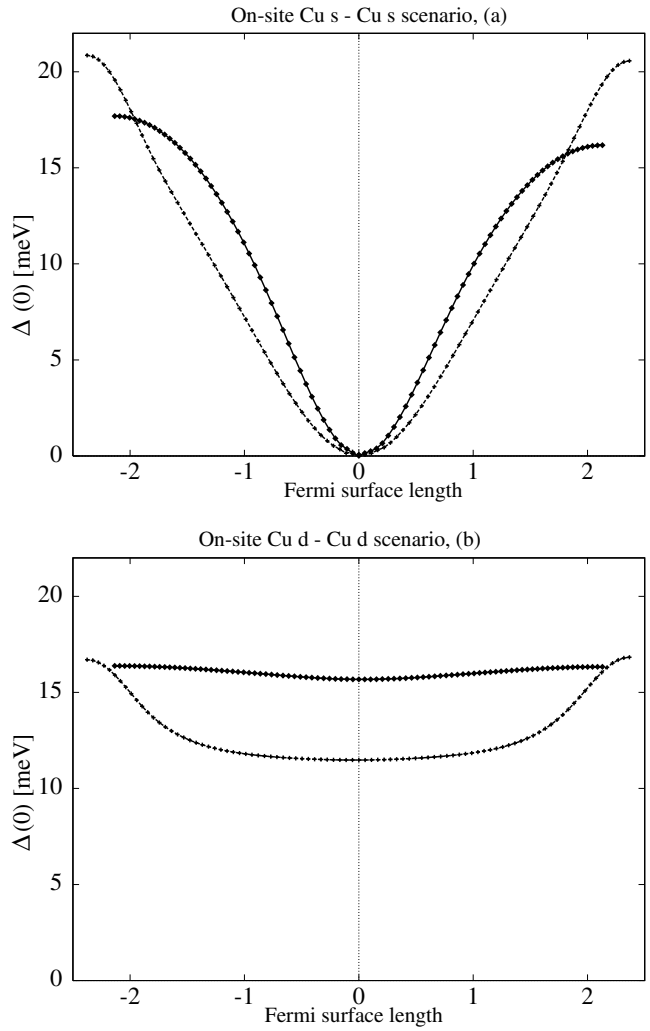

Figure 4. The calculated anisotropy of (half) the gap, for the on-site Cu s–Cu s (a), the on-site Cu $d_{x^2-y^2}$–Cu $d_{x^2-y^2}$ (b), and the on-site Cu s–Cu $d_{x^2-y^2}$ (c), the intra-layer nearest-neighbour Cu s–Cu $d_{x^2-y^2}$ (d), and the intra-layer nearest-neighbour Cu $d_{x^2-y^2}$–Cu $d_{x^2-y^2}$ (e) scenarios, as a function of the Fermi-surface length measured from the crossing with the ΓS line and in units of the inverse lattice constant, for the odd (crosses) and even (diamonds) sheets of the Fermi surface.

of these schematic diagrams is that they explicitly indicate the sites and orbitals that the members of the Cooper pair occupy when they experience an attractive interaction, whose strength K is chosen such that the calculated T_c coincides with the experimentally observed T_c of the optimally doped compound. In the case of YBCO, it is 92 K. Note that the calculated T_c is the lowest temperature for which the pairing amplitude converges to zero.

Among the s-type scenarios two are local and one is non-local. Note that even the local scenarios can lead to a very anisotropic gap as a function of the FS length (see figure 4(a)). The reason for this is that the k-dependence of the gap is determined by both the underlying electronic structure and the k-dependence of the pairing potential, i.e., it is a combined effect of the two. So, even for a local potential the gap can be very anisotropic if the character of the

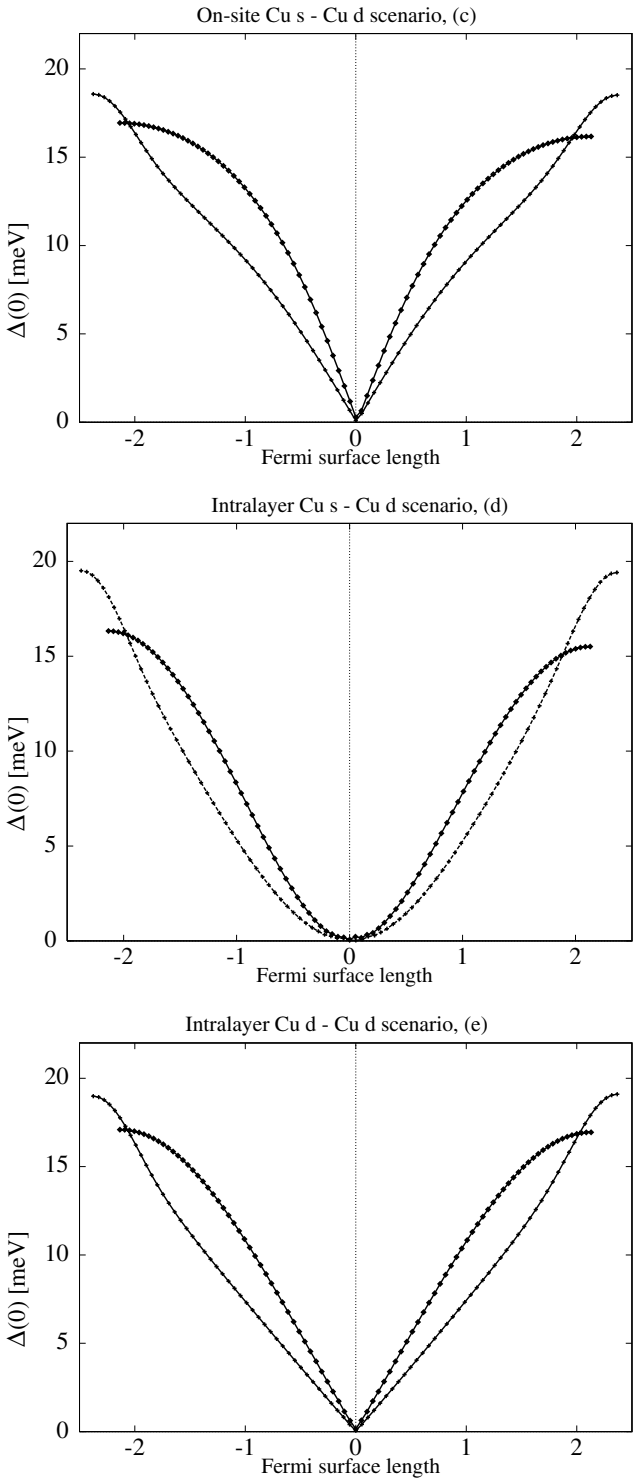

Figure 4. (Continued)

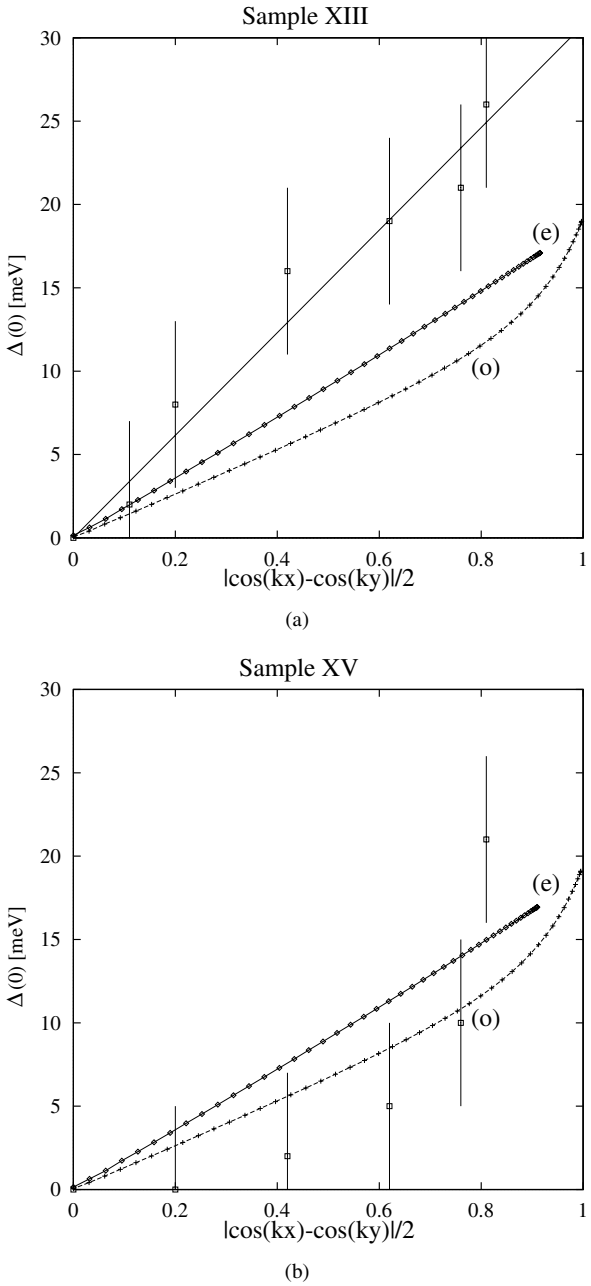

Figure 5. A comparison of the calculated gap for the intra-layer nearest-neighbour Cu $d_{x^2-y^2}$–Cu $d_{x^2-y^2}$, scenario with $K_{dd}(a) = 0.68$ eV for the even (e) and odd (o) sheets of the Fermi surface, with the experimental data deduced by Schabel *et al* [15], from photoemission measurements on their sample XIII (a), sample XV (b), sample XVII (c), and sample XIII 2 (d).

wave-function coefficients varies significantly across the FS. Thus the local scenario, where both members of the Cooper pair reside in the Cu s orbital, belonging to the same Cu site, leads to a very anisotropic gap which however is of the extended s type, with $K_{ss}(0) = 14.3$ eV,

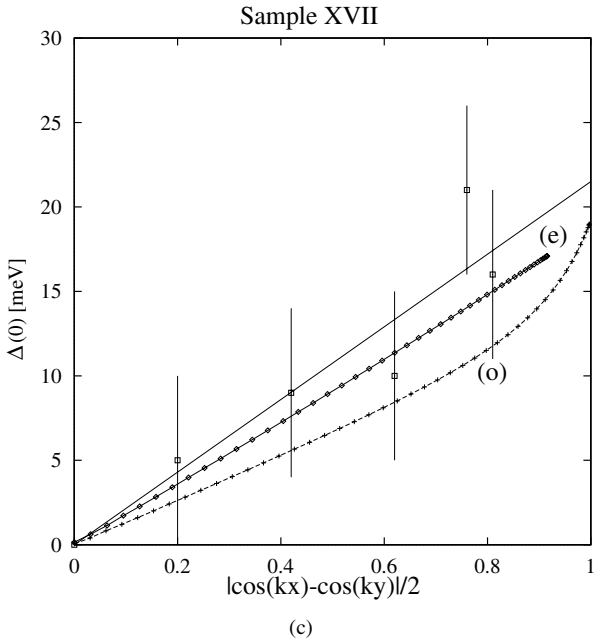

(c)

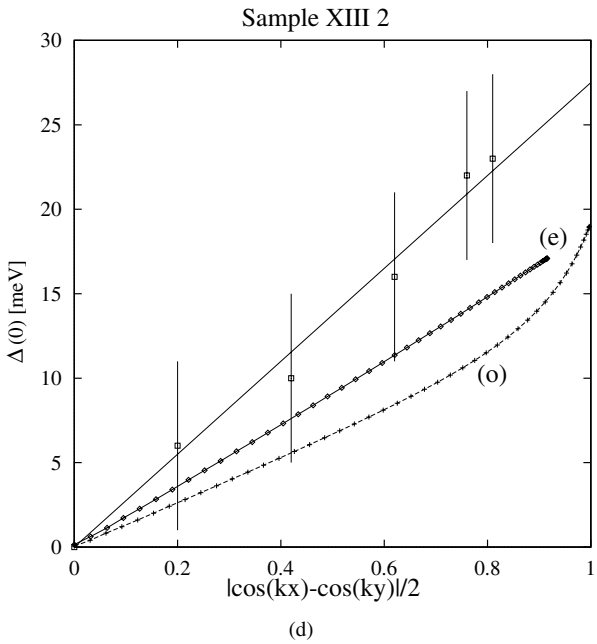

(d)

Figure 5. (Continued)

and its large variation across the Fermi surface reflects strong hybridization of the Cu s with the pdσ anti-bonding band. On the other hand, the local scenario where the members of the Cooper pair occupy Cu $d_{x^2-y^2}$ orbitals on the same site, with $K_{\rm dd}(0) = 1.23$ eV, leads to a very isotropic s-wave gap, very much like the one for the conventional BCS superconductor. The reason for this is that the character of the Cu $d_{x^2-y^2}$ orbital remains fairly constant across the

FS, and there is no contribution from the pairing potential. The last s-type scenario in figure 3 is an example of another case of extended s symmetry (see figure 4(d)). This time, however, it is a combined effect of the variation of the Cu s character across the FS and the lattice Fourier transform of the pairing potential, since the respective orbitals, s and $d_{x^2-y^2}$, belong to the nearest-neighbour copper sites, and the coupling parameter is $K_{sd}(a) = 2.32$ eV, with a being the nearest-neighbour separation.

The two d-wave scenarios that we have studied in considerable detail are shown by the two schematic diagrams at the bottom of figure 3. The one on the left is a local scenario, i.e. the electrons of opposite spins and momenta occupy respectively s and $d_{x^2-y^2}$ orbitals on the same Cu site, with $K_{sd}(0) = 5.25$ eV. The other d-wave scenario, on the bottom right, is non-local with $K_{dd}(0) = 0.68$ eV and the members of the Cooper pair occupying $d_{x^2-y^2}$ orbitals on the nearest-neighbour Cu sites (the intra-layer nearest-neighbour Cu $d_{x^2-y^2}$–Cu $d_{x^2-y^2}$ scenario). One can see that although both lead to a d-wave gap, with well defined cusps at the zero FS length (see figures 4(c) and 4(e)), the respective shapes are slightly different, and in particular the values of the coupling constants $K_{dd}(a)$ and $K_{sd}(0)$ are very different, by nearly an order of magnitude. As mentioned before, the respective gap anisotropies are a combined effect of the underlying electronic structure, represented by the eight-band model, and the lattice Fourier transform of the pairing potential. In the case of the non-local scenario it is nearly entirely the latter that determines the gap anisotropy, since the Cu $d_{x^2-y^2}$ character remains fairly constant across the FS. In the case of the local scenario the k-dependence of the pairing potential does not contribute, and neither does Cu $d_{x^2-y^2}$, whose character hardly changes across the FS. So, the very anisotropic gap is due to the peculiar behaviour of Cu s, and its hybridization with the pdσ Cu–O bands crossing the Fermi level. Since the coupling constant of the local scenario is nearly ten times larger than the one for the non-local scenario, then it is hard to believe that the local scenario would be the one for YBCO.

The general point to make regarding pairing scenarios is that although T_c for all these scenarios is 92 K, the values of the corresponding coupling parameters, measuring the strength of the attractive interaction experienced by the members of the Cooper pair, vary rather substantially. Therefore, if one was to classify these scenarios with respect to the probability of their occurrence, as defined by the size of the interaction constant K, then the Cu s–Cu s local scenario would be least likely, merely on account of the huge coupling constant it requires for the superconductivity to occur. Hence, it is perhaps just a curiosity rather than a real possibility. Since, however, YBCO is reported to be a d-wave superconductor, we need not worry about this. By the same token, the non-local d-wave scenario, with members of the Cooper pair occupying the nearest-neighbour Cu $d_{x^2-y^2}$ orbitals, should be the most favourable scenario. To show that this is indeed the case, in figure 5 we compare the superconducting gap for this d-wave scenario with the ARPES measurements by Schabel *et al* [15]. We plot there both even and odd superconducting gaps as functions of the characteristic k-space dependence of the d-wave order parameter, $|\cos kx - \cos ky|/2$. Note that both even and odd gaps show, as they should, convincing linear dependence. Although our calculations correspond to a T_c of 92 K, we compare against the measurements by Schabel *et al* for all four samples corresponding to different T_cs. And the agreement with our results is fairly satisfactory for all the samples. The error bars are quite large, and the lines through them serve here merely as a guide for the eyes. Nevertheless, the near quantitative agreement with the results for sample XVII can be taken as evidence that the relation between the attractive force, represented by the coupling coefficient $K_{dd}(a)$, and the gap in the quasiparticle spectrum is correctly described by our BdG equations with the eight-band model Hamiltonian. Considering that we did not fit to any feature of the measured gap, but only to obtain $T_c = 92$ K, the agreement is truly amazing. The BCS ratios for all the samples are of the order of 5 to about 8. Our calculated value of 4.8 agrees quite well

with the value of 5.4 for the sample XVII. Regarding the local d-wave scenario we conclude, on the basis of figures 4(c) and 4(e), that its agreement with the experiments by Schabel *et al* will not be as satisfactory.

5.2. Density of states and specific heat

It is well known that d-wave symmetry of the gap implies linear dependence of the density of states around the energy zero, relative to the chemical potential. Although this linearity is a foregone conclusion, the slope is not, and can be verified experimentally e.g. by low-temperature specific heat measurements. And this could differentiate between various scenarios and help in identifying the correct one, shedding light, indirectly, on a possible pairing mechanism. As can be seen in figure 6, the two d-wave scenarios give rise to different slopes of the DOS and similarly lead to different slopes for the low-temperature specific heat (figure 7). The latter has been calculated according to the formula for independent fermions

$$C_v^S(T) = \sum_{\boldsymbol{k}\nu} \frac{\beta}{2T} \left[E_\nu^{\boldsymbol{k}} + \beta \frac{\partial E_\nu^{\boldsymbol{k}}}{\partial \beta} \right] \frac{E_\nu^{\boldsymbol{k}}}{\cosh^2(\beta E_\nu^{\boldsymbol{k}}/2)} \tag{14}$$

with $\beta = 1/k_B T$, where k_B is the Boltzmann constant. Note that the local scenario gives rise to a substantially smaller slope, and accordingly smaller prefactor of the power-law behaviour of the specific heat which is a quadratic function of T/T_c. Specifically, for the non-local d-wave scenario we have calculated the low-temperature electronic specific heat in the superconducting state to follow the relation $C_v^S(T) = 0.93(T/T_c)^2$, while for the local scenario, $C_v^S(T) = 0.63(T/T_c)^2$. What these results tell us is that although the two scenarios have the same T_cs their respective quasiparticle spectra are very different, i.e., the k-dependences of the respective superconducting gap functions, $\Delta^k(T)$, around their nodes, are very different,

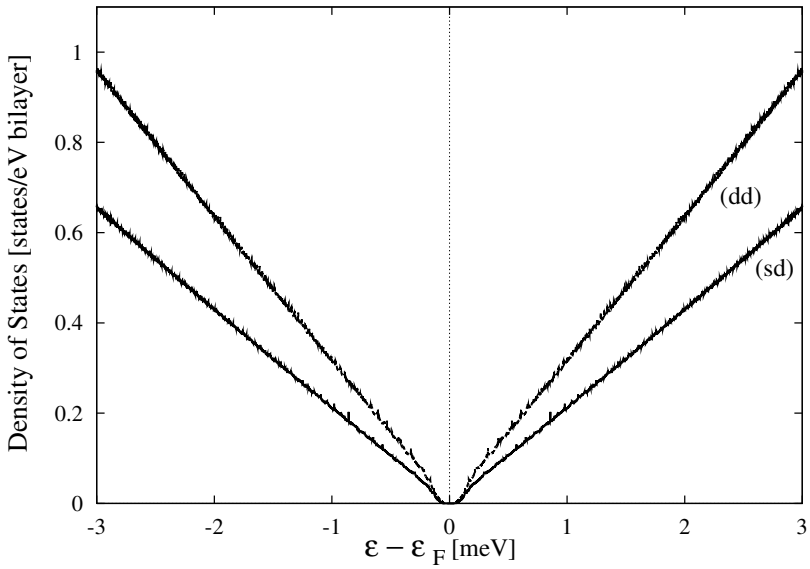

Figure 6. A comparison of the linear behaviour of the total quasiparticle density of states in the vicinity of the chemical potential for two different 'd-wave' pairing scenarios: the intra-layer nearest-neighbour Cu $d_{x^2-y^2}$–Cu $d_{x^2-y^2}$ scenario with $K_{\rm dd}(a) = 0.68$ eV and the on-site Cu s–Cu $d_{x^2-y^2}$ scenario with $K_{\rm sd}(0) = 5.25$ eV.

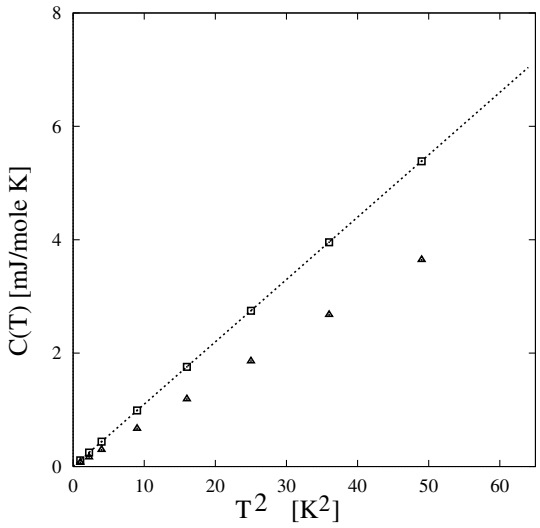

Figure 7. A comparison of the calculated low-temperature electronic specific heat in the superconducting state for two different d-wave scenarios featuring the intra-layer nearest-neighbour Cu $d_{x^2-y^2}$–Cu $d_{x^2-y^2}$ coupling with $K_{dd}(a) = 0.68$ eV (squares) and the on-site Cu s–Cu $d_{x^2-y^2}$ coupling with $K_{sd}(0) = 5.25$ eV (triangles). The dotted curve marks the experimental result of Moler *et al* [16].

and the ways the gaps rise from their nodes in k-space are different. The electronic specific heat is only a small fraction of the total specific heat, and it is extremely difficult to extract from measurements. However, Moler *et al* [16] managed to extract from their experiments the slope coefficient of the low-temperature superconducting electronic specific heat, and it turned out to be in excellent agreement with our result for the non-local d-wave scenario [3], namely they found $C_v^S(T)^{\exp} = 0.95(T/T_c)^2$. Since the linear dependence of the DOS of the d-wave superconductor translates to a power-law (T^2-) dependence of the low-temperature electronic specific heat, this power law is a foregone conclusion, but the slope of the specific heat is a quantitative prediction of the calculation, and it is very satisfying that our result for the non-local d-wave scenario agrees so well with the experiment by Moler *et al* [16].

5.3. Penetration depth and superfluid density

Unlike the specific heat, the penetration depth, λ, has only an electronic contribution and seems to be relatively easy to measure. Also, it holds similar information to the specific heat. Penetration depth at low temperatures is a very important quantity to calculate since it is a direct measure of the superfluid density and hence can hold an important clue to the mechanism of pairing. It is only at low temperatures that the superfluid density is unaffected by a possible presence of low-lying excitations that are not associated with the nodes in the superconducting gap.

Following the semiclassical approach of Chandrasekhar and Einzel [17], the superfluid density tensor has the form

$$\bar{\mathcal{T}} = \mathcal{T} - \frac{(\mathcal{T}\cdot\boldsymbol{q})(\boldsymbol{q}\cdot\mathcal{T})}{\boldsymbol{q}\cdot\mathcal{T}\cdot\boldsymbol{q}} \tag{15}$$

where $\boldsymbol{q}$ is a unit vector in the direction of the current flow, and the second term on the right-hand side is due to the back flow. Furthermore, $\mathcal{T}$ is the difference between the diamagnetic

and paramagnetic contributions:

$$\mathcal{T} = \mathcal{T}^D - \mathcal{T}^P \tag{16}$$

with the diamagnetic ($\mathcal{T}^D$) and paramagnetic ($\mathcal{T}^P$) contributions being

$$\mathcal{T}^D_{\alpha\beta} = \frac{e^2}{4\pi^3 c}\int \mathrm{d}^3k \left(-\frac{\partial n_{\boldsymbol{k}}}{\partial \varepsilon_{\boldsymbol{k}}}\right)(\boldsymbol{v}^\alpha_{\boldsymbol{k}}\boldsymbol{v}^\beta_{\boldsymbol{k}}) \tag{17}$$

and

$$\mathcal{T}^P_{\alpha\beta} = \frac{e^2}{4\pi^3 c}\int \mathrm{d}^3k \left(-\frac{\partial f(E_{\boldsymbol{k}})}{\partial E_{\boldsymbol{k}}}\right)(\boldsymbol{v}^\alpha_{\boldsymbol{k}}\boldsymbol{v}^\beta_{\boldsymbol{k}}). \tag{18}$$

In these formulae the indices α and β stand for x-, y-, and z-axes, e is the electric charge, c is the velocity of light, $\varepsilon_{\boldsymbol{k}}$ and $E_{\boldsymbol{k}}$ are respectively the quasiparticle dispersion relations in the normal and superconducting states,

$$\boldsymbol{v}^\alpha_{\boldsymbol{k}} = \frac{1}{\hbar}\frac{\partial \varepsilon_{\boldsymbol{k}}}{\partial \boldsymbol{k}_\alpha}$$

is the quasiparticle velocity in the α-direction, f is the usual Fermi function, and $n_{\boldsymbol{k}}$ is the occupancy of the single-particle state $\boldsymbol{k}$ in the superconducting state:

$$n_{\boldsymbol{k}} = u^2_{\boldsymbol{k}} f(E_{\boldsymbol{k}}) + v^2_{\boldsymbol{k}}(1 - f(E_{\boldsymbol{k}}))$$

where the amplitudes $u_{\boldsymbol{k}}$ and $v_{\boldsymbol{k}}$ are respectively the quasiparticle and quasihole solutions of the Bogoliubov–de Gennes equations. Note that in the above formulae the band index has been suppressed.

Using the conventional labels a, b, c for the symmetry axes of the layered superconducting cuprates, in the CuO_2 plane, the penetration depths $\lambda_a(T)$ and $\lambda_b(T)$ may be obtained from

$$\lambda_\alpha(T) = \left[\frac{c}{4\pi(\mathcal{T}^D_{\alpha\alpha} - \mathcal{T}^P_{\alpha\alpha})}\right]^{1/2}\Bigg|_{\alpha=a,b}. \tag{19}$$

In figure 8 we show our results, obtained with the above formula, for the relative penetration depth [5], as a function of temperature, for the low-temperature region. The results are for both a- and b-axes (indicating the direction in which currents flow), and both d-wave scenarios, calculated as the difference $\Delta\lambda(T) = \lambda(T) - \lambda(0)$. Our calculations are compared with the measurement of Carrington *et al* [18]. The linear dependence of $\Delta\lambda(T)$ on temperature is due to nodes in the superconducting gap but slopes reflect the quasiparticle spectra, and as before should be a decisive factor for the choice of the most likely scenario for YBCO.

Note that in the excluded-volume technique, used by Carrington *et al*, the measured curves start at 1.4 K, since this is the lowest temperature that can be resolved. Moreover, the experiment measures only the relative quantity $\Delta\lambda(T)$. What is measured is the effective shielding volume of the sample penetrated by the magnetic field. Therefore, no information on the absolute $\lambda(0)$ can be obtained from this technique. One thing to observe here is that the calculated relative penetration depth shows no anisotropy between a- and b-quantities. In this respect the experimental curves also hardly differ from one another. Although all curves are convincing straight lines, their slopes are substantially different, and it looks like the favoured d-wave scenario is not as good as the local scenario. This, however, seems to be due to the fact that in the eight-band model we only have two FS sheets (figure 2(c)), while for the penetration depth at $T = 0$ K the whole FS is of importance. Thus our quantities are underestimated, and due to the lack of the chain FS sheet our $\lambda(0)$s for the a- and b-directions are very much the same, namely $\lambda_a(0) = 1883$ Å and $\lambda_b(0) = 1839$ Å. That the chain matters is supported by the measurement of Basov *et al* [19] who, using the far-infrared (FIR) spectroscopy, got

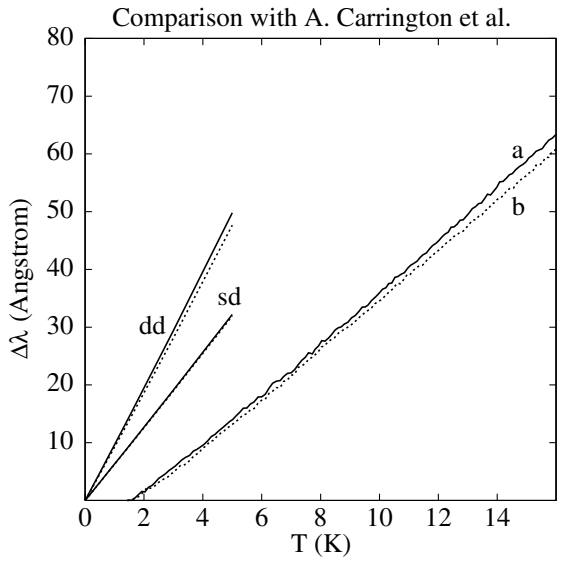

Figure 8. The temperature dependence of the relative penetration depth, $\Delta\lambda_{a\,(b)}(T) = \lambda_{a\,(b)}(T) - \lambda_{a\,(b)}(0)$ (Å), as calculated on the basis of the eight-band model for the intra-layer nearest-neighbour Cu $d_{x^2-y^2}$–Cu $d_{x^2-y^2}$ scenario (dd) and the on-site Cu s–Cu $d_{x^2-y^2}$ scenario (sd). Full curves correspond to the a-axis and the dotted curves to the b-axis. Here the results obtained by Carrington *et al* [18] are plotted for comparison.

widely different values for the two quantities, indicating that superconductivity extends also to the chains. From the Basov *et al* measurement, $\lambda_a(0) = 1600$ Å is substantially larger than $\lambda_b(0) = 1200$ Å, implying that the chain seems to enhance the superfluid density.

To interpret the experimental data of Carrington *et al* [18] in terms of the superfluid density one needs $\lambda(0)$ both for a- and b-directions. Since, as mentioned before, Carrington *et al* could not measure the absolute quantities, the values of Basov *et al* have been used. As one can see in figure 9, the experimental curves for both a- and b-directions, although linear, are very different from one another, showing large anisotropy between them. Remembering that the relative penetration depth has been very much the same for both directions, one can conclude that the observed anisotropy is entirely due to the anisotropy between $\lambda_a(0)$ and $\lambda_b(0)$. Contrary to the experimental result, the calculated curves show no noticeable difference between the two directions and again the Cu s–Cu $d_{x^2-y^2}$ local scenario agrees better with the experiment (figure 9(b)) than the other d-wave scenario (see figure 9(a)). As mentioned before, the reason for this is that our calculation for $\lambda(0)$ gives very much the same values for the two directions, which is due to the lack of the chain in the eight-band model. This is clearly demonstrated in figure 10, where we compare our calculation for the non-local scenario of the superfluid density with the measurement by Carrington *et al*, but this time for $\lambda_a(0)$ and $\lambda_b(0)$ we have used the results of Basov *et al*, while for the other temperatures the calculated $\lambda_a(T)$ and $\lambda_b(T)$ have been used. One can see that, similarly to the case for the experimental curves, we now observe a large anisotropy between the two different directions. This is then a demonstration that the eight-band model is not sufficient for the penetration depth calculation, and that the chain contributes to the superfluid density quite substantially.

In this way, we have exhausted reviewing our results for the optimally doped compound. Since our results compared rather favourably with experiments, in the remaining part of the results section we shall concentrate on the calculations for different doping levels.

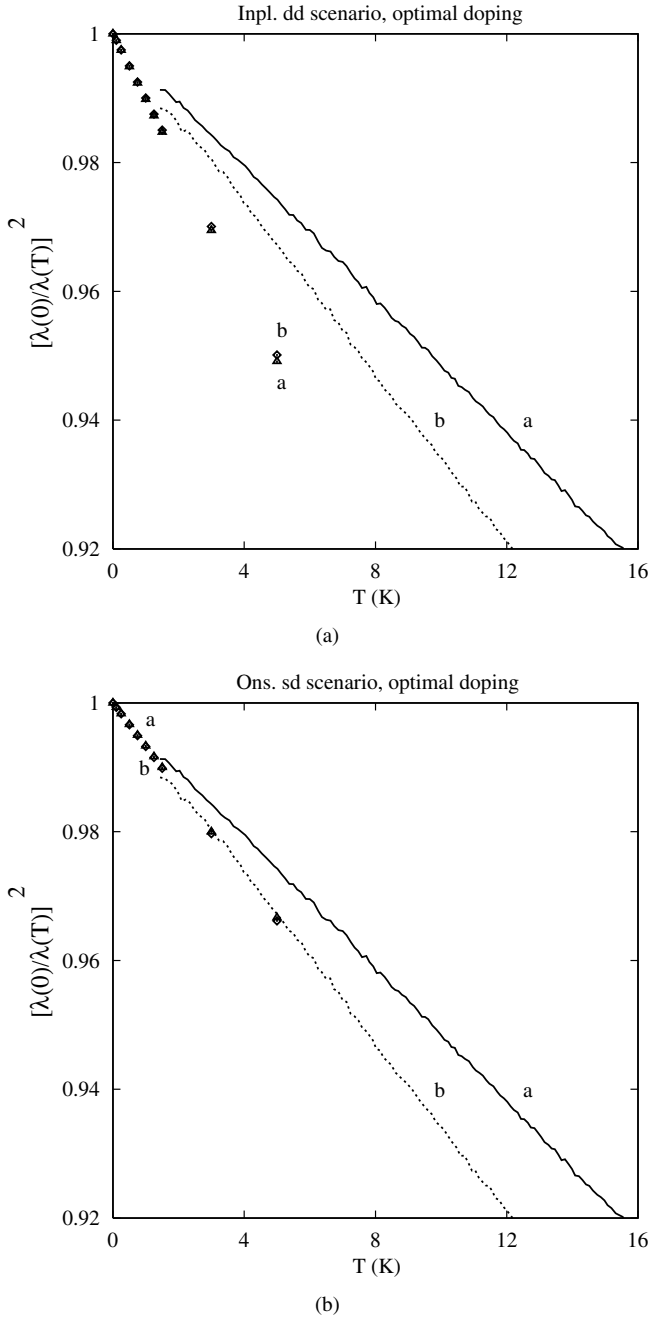

Figure 9. (a) The temperature dependence of $(\lambda_{a\,(b)}(0)/\lambda_{a\,(b)}(T))^2$, the calculated superfluid density, for the intra-layer nearest-neighbour Cu $d_{x^2-y^2}$–Cu $d_{x^2-y^2}$ scenario, in comparison with the results of Carrington *et al* [18] ('Inpl.' is standing for 'In-plane'). In the theoretical results, triangles correspond to the *a*-axis and the diamonds to the *b*-axis. (b) The temperature dependence of the calculated superfluid density, $(\lambda_{a\,(b)}(0)/\lambda_{a\,(b)}(T))^2$, for the on-site Cu s–Cu $d_{x^2-y^2}$ scenario, in comparison with the results of Carrington *et al* [18] ('Ons.' is standing for 'On-site'). In the theoretical results, triangles correspond to the *a*-axis and the diamonds to the *b*-axis.

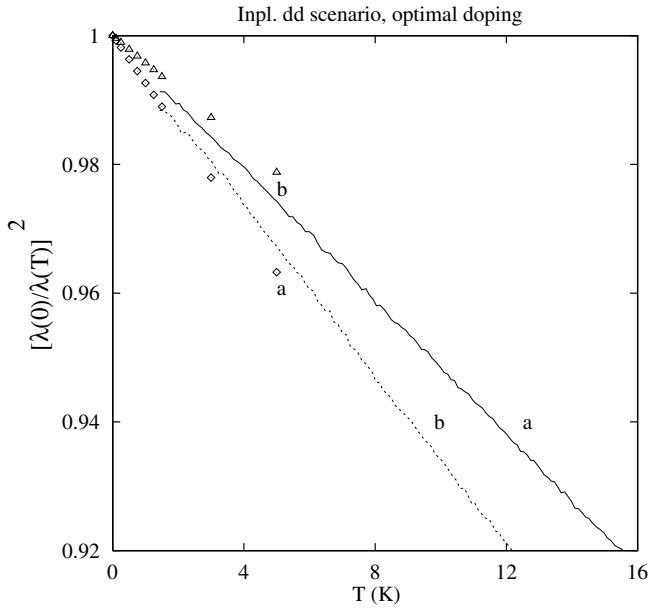

Figure 10. The temperature dependence of the calculated superfluid density, $(\lambda_{a\,(b)}(0)/\lambda_{a\,(b)}(T))^2$, for the intra-layer nearest-neighbour Cu $d_{x^2-y^2}$–Cu $d_{x^2-y^2}$ scenario, with $\lambda_{a\,(b)}(0)$ taken from the measurement of Basov *et al* [19]. For comparison, the relevant experimental data of Carrington *et al* [18] are also displayed. In the theoretical results, the diamonds correspond to the a-axis and the triangles correspond to the b-axis.

5.4. Doping dependence of T_c

Assuming that neither the attractive interaction, in terms of the coupling coefficient $K_{LL'}$, nor the tight-binding parameters of the eight-band model change much with doping, we have studied T_c as a function of doping.

Different levels of doping have been accomplished by changing the chemical potential in the BdG equations, but the tight-binding parameters of the eight-band model and the coupling constant K have been kept at the values derived for the optimally doped YBCO with $T_c = 92$ K. Our results for two different pairing scenarios, namely the isotropic s wave and the favourable, non-local d wave, are shown in figure 11(a). In figure 11(b) we show the experimental universal curve of T_c versus doping, for a large number of high-T_c superconductors [14]. Note that the experimental points of figure 11(b), corresponding to YBCO (123 compound), have also been plotted in figure 11(a) for comparison. What is seen here is that T_c rises and then falls as one moves from the overdoped to the underdoped region, and the maximum is at the optimally doped compound. The calculated curves reflect the rise and fall of T_c as one moves from below to above the VHS peak in the density of states, thus indicating the importance of the VHS for the high-T_c superconductivity. According to the Van Hove scenario [14], a VHS could enhance any weak-coupling interaction, leading to large values of T_c.

When comparing our calculations with the experimental data, one can see that both scenarios can reproduce very well the observed rise and fall of T_c with doping. However, what is rather amazing is that the width of the non-local scenario curve at half-maximum compares very favourably with that of the universal curve, namely 0.14 holes/layer versus 0.15 holes/layer. The observed asymmetry of the theoretical curves is due to the bifurcated saddle points. In fact, one can also see some asymmetry in the experimental points for YBCO

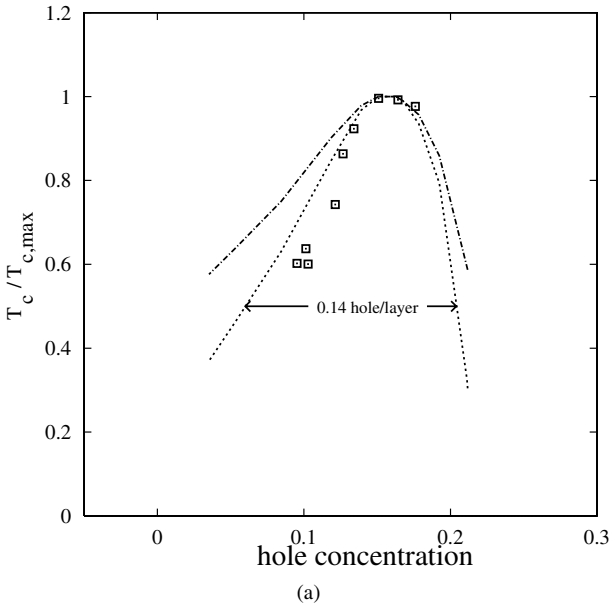

(a)

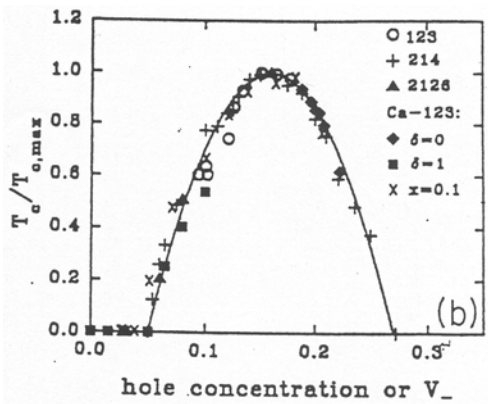

Figure 11. (a) T_c, normalized to the value at optimal doping, $T_{c,max}$, versus hole concentration for the CuO_2 bilayer of $YBa_2Cu_3O_7$. The dotted curve corresponds to the intra-layer nearest-neighbour Cu $d_{x^2-y^2}$–Cu $d_{x^2-y^2}$ scenario (d wave), while the dash–dotted curve represents the on-site Cu $d_{x^2-y^2}$–Cu $d_{x^2-y^2}$ scenario (s wave). The squares are the experimental points for $YBa_2Cu_3O_7$, extracted from (b), the universal curve of T_c versus hole concentration [14].

(figure 11(a)). The fast fall of the theoretical curve on the overdoped side is due to the loss of the electron pockets at the X and Y points when moving the chemical potential down, well below the VHS peaks. By moving the chemical potential down below the Fermi level, the FS recedes from the d-rich regions of space.

5.5. T_c versus $1/\lambda^2(0)$

As can be seen in figure 12, for the non-local d-wave scenario and both a- and b-axes, $1/\lambda^2(0)$ also shows a rise and fall as a function of doping. Here, however, unlike in the case of T_c versus doping, the maximum is not at the optimal doping, for reasons discussed when we presented

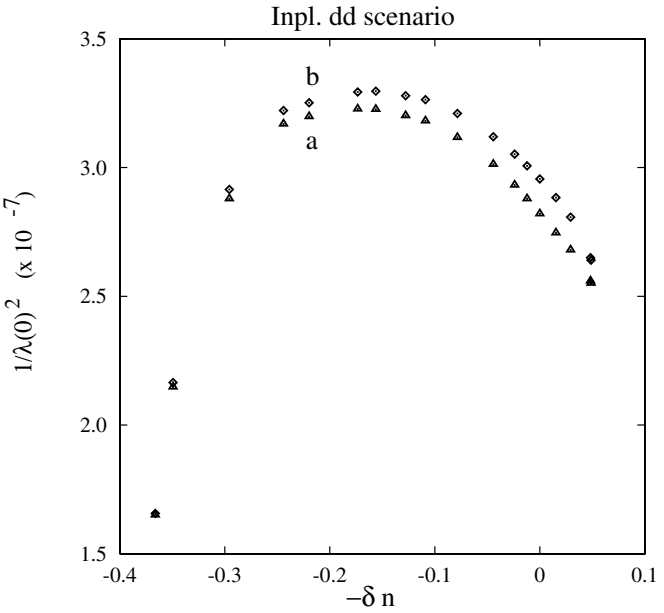

Figure 12. The calculated dependence of $1/\lambda(0)^2$ (in Å^{-2}) on the deviation of the number of holes from that at optimal doping for the CuO_2 bilayer of $YBa_2Cu_3O_7$ for the intra-layer nearest-neighbour Cu $d_{x^2-y^2}$–Cu $d_{x^2-y^2}$ scenario. The triangles correspond to the a-axis and the diamonds to the b-axis.

the penetration depth results at optimal doping. Nevertheless, one can try to extract from T_c versus doping, together with $1/\lambda^2(0)$ versus doping, the T_c versus $1/\lambda^2(0)$ dependence, and this is shown in figure 13, for both a- and b-axes and the favourable d-wave scenario only. This dependence reflects similar behaviour to what is usually referred to as the Uemura plot [20] of T_c versus σ (the muon spin-relaxation rate which is believed to be proportional to $1/\lambda^2(0)$, since it is proportional to n_S/m^*, with n_S and m^* being respectively the superfluid carrier density and the effective electron mass). What the calculated curves show is a kind of a boomerang effect. In fact, the shape of the curves is very similar to the curve plotted by Markiewicz [14] for DOS(ε_F) against the square of the plasma frequency, which is the expected behaviour near the VHS. The Uemura plot constitutes substantial and intriguing evidence that T_c and $1/\lambda_\alpha^2(0)$ rise and fall together as we dope from below to above the optimal concentration of holes $\delta n = 0$. Since our calculations resemble this behaviour, we are in the position of being able to identify a mechanism which is responsible for this universally observed T_c versus $1/\lambda_\alpha^2(0)$ relationship. Evidently, to the extent that our model captures the essential physics of the superconducting YBCO, it is due to the presence of a Van Hove-like bifurcated saddle point in the electronic structure featured by the eight-band model.

5.6. Doping dependence of the superfluid density

In figure 14, we present the doping dependence of the superfluid density for the non-local d-wave scenario and five different levels of doping, as a function of the relative temperature. In figure 15, for comparison, we show the measurements after Hardy *et al* [21], for the whole temperature range up to T_c, for three different doping levels, producing evidence that $\lambda_{a\,(b)}^2(0)/\lambda_{a\,(b)}^2(T)$ is an almost universal function of T/T_c in the sense that the data for different

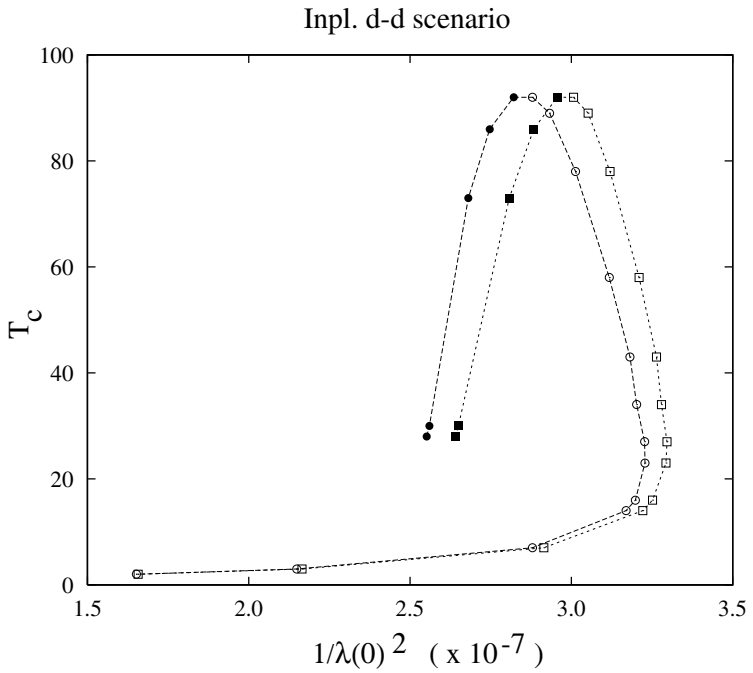

Figure 13. The calculated T_c (in K) versus $1/\lambda^2(0)$ (in Å^{-2}) for the intra-layer nearest-neighbour Cu $d_{x^2-y^2}$–Cu $d_{x^2-y^2}$ scenario along both the a-direction (circles) and b-direction (squares). Here the full symbols correspond to the overdoped compounds and the open symbols to the underdoped compounds. The connecting lines serve as a guide for the eyes.

levels of doping fall more or less on the same curve for the whole temperature range up to T_c. Note that the respective axes for the calculated curves run only from 0 to 0.12 and from 0.86 to 1.00. In contrast, the experimental data run over 0.0 to 1.00 in both cases. Unfortunately, to calculate for the whole temperature range would have been quite tricky, especially as regards performing the BZ integration in the full BZ without having the full FS which matters a lot for $\lambda_{a\,(b)}(0)$.

There are a couple of points that we would like to make regarding the calculated curves. First is that we do not see much variation as a function of doping, in agreement with the experiment. Our results, displayed in figure 14, for the intra-layer Cu $d_{x^2-y^2}$–Cu $d_{x^2-y^2}$ scenario, are clearly consistent with these facts: a 21% change in T_c from the optimal to an overdoped compound ($T_c = 73$ K), corresponding to a relative change in the band filling per layer of 0.03, results in an 8% change in the superfluid density tensor $\lambda_\alpha^2(0)/\lambda_\alpha^2(T)$ for both a- and b-directions. For the underdoped compounds a change of 15% in T_c, equivalent to a relative change in the band filling per layer of about -0.04, leads to a 3% change in the superfluid density tensor $\lambda_\alpha^2(0)/\lambda_\alpha^2(T)$ for the a-direction and a 2% change for the b-direction (see table 1). This again indicates that changing the band filling, without altering either the electron–electron interaction constant or the energy bands of the normal states, is capable of accounting for the striking variations of many superconducting properties.

The calculated superfluid density curves reflect the VHS in that the optimally doped curve lies in the middle, and those of the other doping levels on the respective sides of it. Moreover, as in the case of the optimally doped compound, the calculated $\lambda(0)$s do not show much variation, both between a- and b-directions, and as a function of doping. Different observations can be

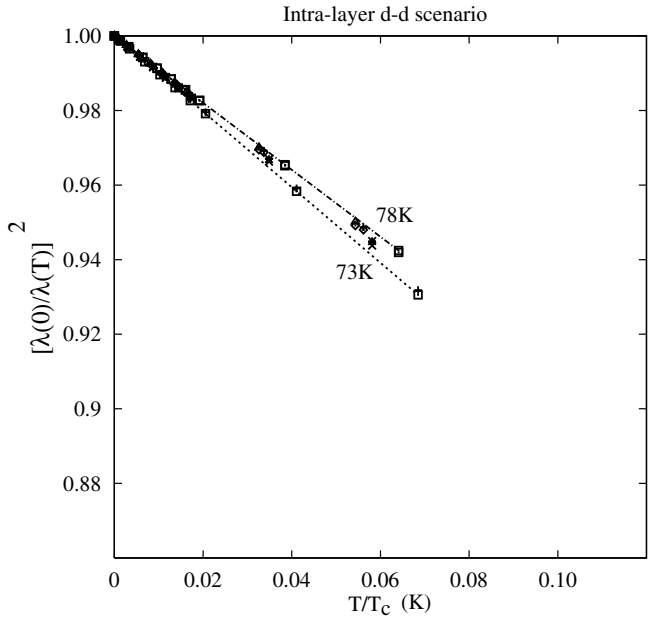

Figure 14. The calculated superfluid density, $(\lambda_{a\,(b)}(0)/\lambda_{a\,(b)}(T))^2$, as a function of T/T_c, for a- and b-axes and five different band fillings for the CuO_2 bilayer of $YBa_2Cu_3O_7$, and the intra-layer nearest-neighbour Cu $d_{x^2-y^2}$–Cu $d_{x^2-y^2}$ scenario. The calculated curves correspond respectively to two overdoped compounds with $T_c = 73$ K and 86 K, the optimally doped compound with $T_c = 92$ K, and two underdoped compounds with $T_c = 78$ K and 89 K. The dotted and chain curves drawn through the calculated points correspond to the overdoped compound with $T_c = 73$ K and the underdoped compound with $T_c = 78$ K. All of the calculated results are enclosed in between these two outermost curves, with a very small variation in the slopes, and also reflecting the Van Hove singularity in the calculated electronic structure. The results for the optimal doping fall exactly in the middle of the region enclosed by the two outermost curves. The results for the underdoped compounds lie to the right of the optimal doping results and the ones for the overdoped compounds to the left.

Table 1. The change of the superfluid density slope, defined as $S = \mathrm{d}x/\mathrm{d}t$, with $x = (\lambda_{a\,(b)}(0)/\lambda_{a\,(b)}(T))^2$ and $t = T/T_c$, as a function of doping. Also the doping dependences of $\lambda_a(0)$ and $\lambda_b(0)$ are presented. The calculated values correspond to two underdoped compounds with $T_c = 78$ K and 89 K, the optimally doped compound with $T_c = 92$ K, and two overdoped compounds with $T_c = 73$ K and 86 K.

T_c (K)	Compound	a-axis	b-axis	$\lambda_a(0)$ (Å)	$\lambda_b(0)$ (Å)
78	Underdoped	−1.014	−0.995	1822	1790
89	Underdoped	−0.967	−0.946	1847	1810
92	Optimal	−0.936	−0.918	1883	1839
86	Overdoped	−0.926	−0.913	1908	1862
73	Overdoped	−0.906	−0.898	1931	1887

made looking at table 2, where the respective experimental quantities are quoted. This again is due to the lack of the full FS in the eight-band model used in the calculations. We believe that including the chain-related Fermi-surface sheet would not only increase the anisotropy between $\lambda_a(0)$ and $\lambda_b(0)$, but could also reverse their ascending order to the descending one, when moving from underdoped to overdoped compounds, in agreement with experiment [22].

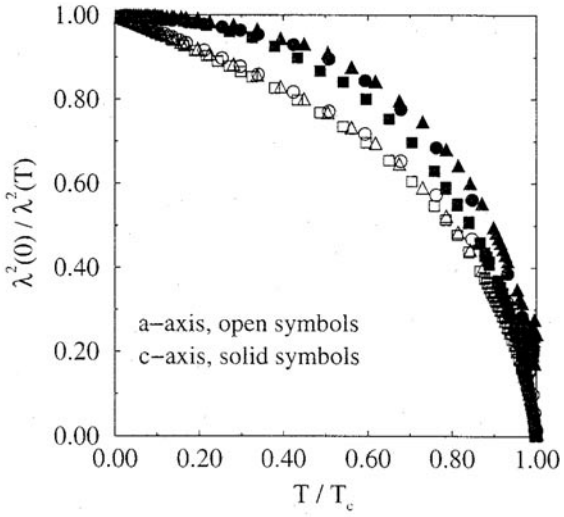

Figure 15. The superfluid density, $(\lambda_{a\,(c)}(0)/\lambda_{a\,(c)}(T))^2$, as a function of T/T_c, from Hardy *et al* [21] for $YBa_2Cu_3O_x$ with $x = 6.6$ (circles, 6.95 (squares), and 6.99 (triangles), showing near universal behaviour versus doping.

Table 2. The experimental values of $\lambda_a(0)$ and $\lambda_b(0)$ for three different doping levels as reported in the review article by Hardy *et al* [21]. The asterisk marking the values for the overdoped compound means that these values were obtained by extrapolation from the results for the optimally doped compound, and are not an outcome of a measurement.

T_c (K)	Compound	$\lambda_a(0)$ (Å)	$\lambda_b(0)$ (Å)
89.0	Overdoped	1600*	800*
93.2	Optimal	1600	1030
59.0	Underdoped	2100	1600

5.7. Doping dependence of the superconducting gap

In figure 16 we show the calculated doping dependence of the superconducting gap for the non-local d-wave scenario [6]. Like in the case of the study of T_c versus doping, different levels of doping have been accomplished by changing the chemical potential in the BdG equations, but neither the tight-binding parameters of the eight-band model nor the coupling constant K have been updated during the self-consistency cycles. They have been kept at the values derived for the optimally doped YBCO compound with $T_c = 92$ K.

Surprisingly our results, both for the odd and even sheets of the FS, agree qualitatively with the lower of the two energy scales identified in a recent report by Deutscher [23]. Deutscher arrived at these two energy scales in the superconducting state, Δ_p and Δ_c, by comparing gap energies, measured by different experimental techniques well below T_c, for various copper oxide superconductors. Δ_p, determined either by ARPES or tunnelling spectroscopy, is associated with the single-particle excitation energy, namely the energy per particle required to split the paired charge carriers that are required for superconductivity. Δ_c, determined mainly by Andreev reflection experiments, is associated with the coherence energy range of the superconducting state, i.e., the macroscopic quantum condensate of the paired charges. In the overdoped regime the two energy scales converge to approximately the same value, as

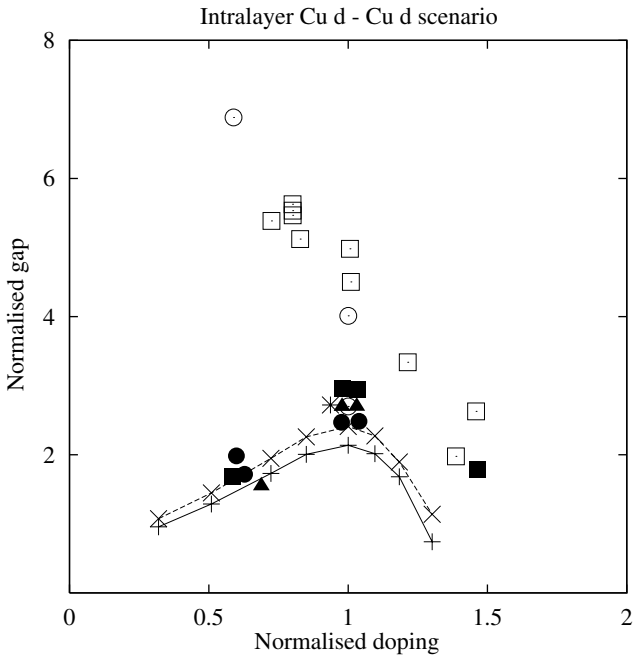

Figure 16. The calculated superconducting gap for both even (solid curve with plus signs) and odd (dashed curve with crosses) sheets of the Fermi surface of YBCO, as derived from the eight-band model with the intra-layer nearest-neighbour Cu $d_{x^2-y^2}$–Cu $d_{x^2-y^2}$ scenario, in comparison with experimental data reported by Deutscher (see reference [18]). The energy gap values Δ are normalized to $kT_{c,M}$, where M refers to the optimal T_c. The normalized gap is plotted as a function of doping normalized to the optimal doping level. Here circles refer to $YBa_2Cu_3O_{7-\delta}$, squares to $Bi_2Sr_2CaCu_2O_{8+\delta}$, triangles to $La_{2-x}Sr_xCuO_4$, and the star to $HgBa_2CaCu_2O_{6+\delta}$. The open symbols come from the ARPES and tunnelling experiments, while the full symbols refer to the Andreev, penetration depth, and Raman experiments. Additionally to the experimental values collected by Deutscher, in this figure we have also given the value corresponding to the ARPES experiment by Schabel *et al* [15] (see the open circle within the coherence energy scale at the optimal doping).

would be the case for a BCS superconductor, where pairs form and condense simultaneously. Also, since the gap for the optimally doped YBCO, as measured by Schabel *et al* [15], lies in the coherence energy range, one can conclude that the optimally doped YBCO is in the BCS condensation regime. In the underdoped regime, the two energy scales diverge, with Δ_p becoming much larger than Δ_c, and increasing with doping, δn, whilst Δ_c decreases like T_c with δn. It implies that in the underdoped region the superfluid condensation is not in the BCS limit, because Δ_p diverges. The underdoped region is where a pseudogap in the electron excitation spectrum is observed well above T_c [25]. Unfortunately, our methodology does not include any mechanism for describing the pseudogap. Thus, we have concluded that the coherence energy range Δ_c, measured by Andreev reflection, penetration depth, and Raman experiments, is a BCS-like, weak-coupling, superconducting d-wave energy gap. Since with regard to the other energy scale Δ_p our theory has nothing to contribute, we suggest that it is not a superconducting feature of the spectra. This conclusion seems to be supported by recent findings of the intrinsic tunnelling spectroscopy by Krasnov *et al* [24]. These authors have been able to distinguish between the two coexisting gaps in the tunnelling DOS by observing strikingly different magnetic field (H) and temperature (T) dependencies for the two gaps:

(i) the superconducting gap which closes both as H goes to $H_{c2}(T)$ and as T goes to T_c and (ii) the non-superconducting (c-axis) pseudogap, which does not change either with H or T. This speaks against the pseudogap having any relation to superconductivity and eliminates the precursor superconductivity in relation to the pseudogap.

6. Conclusions

We have presented some evidence that the semiphenomenological approach for calculating quasiparticles for high-T_c superconductors works very well for YBCO. Also, our studies indicate that whatever the mechanism, it seems to operate between electrons with opposite spins and momenta on nearest-neighbour Cu sites in $d_{x^2-y^2}$ orbitals. It is important to remember that d-wave symmetry of the gap was not assumed here in any way. It was a result of a combined effect of the underlying electronic structure of the eight-band model and the choice of the pairing interaction represented here by $K_{dd}(a) = 0.68$ eV. Our results seem to indicate that YBCO behaves like a BCS weak-coupling superconductor. All the strong-coupling effects, responsible for making the parent compounds of the high-T_c cuprates bad metals, appear to have gone to creating the exotic pairing, while all the other properties seem to be very much like in the conventional superconductors. Thus, the high-T_c superconductivity appears to be fairly conventional except for the high critical temperature and d-wave pairing.

References

[1] Bednorz J G and Müller K A 1986 *Z. Phys.* B **64** 189
[2] Temmerman W M, Szotek Z, Gyorffy B L, Andersen O K and Jepsen O 1996 *Phys. Rev. Lett.* **76** 307
[3] Gyorffy B L, Szotek Z, Temmerman W M, Andersen O K and Jepsen O 1998 *Phys. Rev.* B **58** 1025
[4] Szotek Z, Gyorffy B L, Temmerman W M and Andersen O K 1998 *Phys. Rev.* B **58** 522
[5] Szotek Z, Gyorffy B L and Temmerman W M 2000 *Phys. Rev.* B **62** 3997
[6] Szotek Z, Gyorffy B L and Temmerman W M 2001 *Physica* C **353** 23
[7] Oliveira L N, Gross E K U and Kohn W 1988 *Phys. Rev. Lett.* **60** 2430
[8] Kohn W, Gross E K U and Oliveira L N 1989 *J. Physique* **50** 2601
[9] Andersen O K, Liechtenstein A I, Jepsen O and Paulsen F 1995 *J. Phys. Chem. Solids* **56** 1573
Andersen O K, Jepsen O, Liechtenstein A I and Mazin I I 1994 *Phys. Rev.* B **49** 4145
[10] Dreizler R M and Gross E K U 1990 *Density Functional Theory* (Berlin: Springer)
[11] Jones R O and Gunnarsson O 1989 *Rev. Mod. Phys.* **61** 689
[12] Suvasini M B, Temmerman W M and Gyorffy B L 1993 *Phys. Rev.* B **48** 1202
[13] Gross E K U, Marques M, Lüders M and Fast L 2001 *Density Functional Theory and its Applications to Materials* vol 577, ed V Van Doren (New York: American Institute of Physics)
[14] Markiewicz R S 1997 *J. Phys. Chem. Solids* **58** 1179
[15] Schabel M C, Park C H, Matsuura A, Shen Z-X, Bonn D A, Liang Ruixing and Hardy W N 1997 *Phys. Rev.* B **55** 2796
[16] Moler K A, Baar D J, Urbach J S, Liang Ruixing, Hardy W N and Kapitulnik A 1994 *Phys. Rev. Lett.* **73** 2744
[17] Chandrasekhar B S and Einzel D 1993 *Ann. Phys., Lpz.* **2** 535
[18] Carrington A *et al* 1999 *Phys. Rev.* B **59** R14 173
[19] Basov D N, Liang R, Bonn D A, Hardy W N, Dabrowski B, Quijada M, Tanner D B, Rice J P, Ginsberg D M and Timusk T 1995 *Phys. Rev. Lett.* **74** 598
[20] Uemura Y *et al* 1991 *Phys. Rev. Lett.* **66** 2665
Uemura Y *et al* 1998 *Phys. Rev.* B **38** 909
[21] Hardy W N, Kamal S and Bonn D A 1998 *The Gap Symmetry and Fluctuations in High T_c Superconductors* ed J Bok *et al* (New York: Plenum)
[22] Tallon J L, Bernhard Ch and Niedermyer Ch 1997 *Supercond. Sci. Technol.* **10** A38
[23] Deutscher G 1999 *Nature* **397** 410
[24] Krasnov *et al* 2000 *Preprint* cond-mat/0006479

[25] Batlogg B 1991 *Phys. Today* **44** 44
Alloul H, Ohno T and Mendels P 1989 *Phys. Rev. Lett.* **63** 1700
Williams G V M *et al* 1997 *Phys. Rev. Lett.* **78** 721
Puchkov A V *et al* 1996 *Phys. Rev. Lett.* **77** 3212
Rossat-Mignod J *et al* 1991 *Physica* B **169** 58
Hwang H Y *et al* 1994 *Phys. Rev. Lett.* **72** 2636
Batlogg B *et al* 1994 *Physica* C **235** 130
Loram J W *et al* 1993 *Phys. Rev. Lett.* **71** 1740
Tallon J L *et al* 1995 *Phys. Rev. Lett.* **75** 4114
Liang W Y *et al* 1996 *Physica* C **263** 277
Nemetschek R *et al* 1997 *Phys. Rev. Lett.* **78** 4837